RAN Resource Usage Prediction for a 5G Slice Broker

Craig Gutterman[†], Edward Grinshpun[‡], Sameer Sharma[‡], Gil Zussman[†]

[†]Electrical Engineering, Columbia University, [‡]Nokia Bell Labs

ABSTRACT

Network slicing will allow 5G network operators to offer a diverse set of services over a shared physical infrastructure. We focus on supporting the operation of the Radio Access Network (RAN) slice broker, which maps slice requirements into allocation of Physical Resource Blocks (PRBs). We first develop a new metric, REVA, based on the number of PRBs available to a single Very Active bearer. REVA is independent of channel conditions and allows easy derivation of an individual wireless link's throughput. In order for the slice broker to efficiently utilize the RAN, there is a need for reliable and short term prediction of resource usage by a slice. To support such prediction, we construct an LTE testbed and develop custom additions to the scheduler. Using data collected from the testbed, we compute REVA and develop a realistic time series prediction model for REVA. Specifically, we present the X-LSTM prediction model, based upon Long Short-Term Memory (LSTM) neural networks. Evaluated with data collected in the testbed, X-LSTM outperforms Autoregressive Integrated Moving Average Model (ARIMA) and LSTM neural networks by up to 31%. X-LSTM also achieves over 91% accuracy in predicting REVA. By using X-LSTM to predict future usage, a slice broker is more adept to provision a slice and reduce over-provisioning and SLA violation costs by more than 10% in comparison to LSTM and ARIMA.

CCS CONCEPTS

• Networks → Wireless access points, base stations and infrastructure; • Computing methodologies → Neural networks;

KEYWORDS

Mobile Traffic Forecasting, Deep Learning

ACM Reference Format:

Craig Gutterman, Edward Grinshpun, Sameer Sharma, Gil Zussman 2019. RAN Resource Usage Prediction for a 5G Slice Broker. In *The Twentieth ACM International Symposium on Mobile Ad Hoc Networking and Computing (Mobihoc '19), July 2–5, 2019, Catania, Italy.* ACM, New York, NY, USA, 10 pages. https://doi.org/10.1145/3323679.3326521

1 INTRODUCTION

It is expected that 5G networks will support a variety of services including smart cities, autonomous and network assisted driving,

Permission to make digital or hard copies of all or part of this work for personal or classroom use is granted without fee provided that copies are not made or distributed for profit or commercial advantage and that copies bear this notice and the full citation on the first page. Copyrights for components of this work owned by others than ACM must be honored. Abstracting with credit is permitted. To copy otherwise, or republish, to post on servers or to redistribute to lists, requires prior specific permission and/or a fee. Request permissions from permissions@acm.org.

Mobihoc '19, July 2–5, 2019, Catania, Italy © 2019 Association for Computing Machinery. ACM ISBN 978-1-4503-6764-6/19/07...\$15.00 https://doi.org/10.1145/3323679.3326521

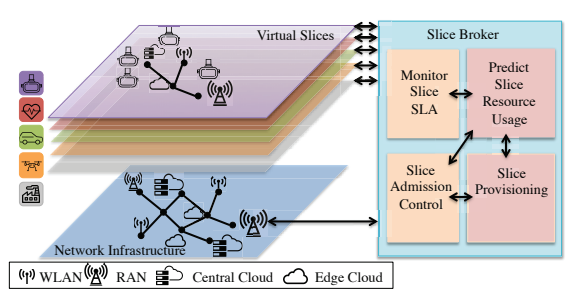


Figure 1: 5G network slice architecture: the network infrastructure is divided into slices for tenants. The RAN broker monitors each slice's SLA. The broker then predicts future slice resource usage. Slice provisioning is done based on the SLA and the predicted resource usage. The slice prediction and provisioning information is used by the slice broker for admission control decisions.

augmented reality, and virtual reality. Such services will impose an extremely diverse set of requirements on the mobile network, ranging from ultra high throughput to ultra low latency at the order of milliseconds [14].

Network slicing will allow 5G operators to split a shared physical infrastructure into virtual slices to meet these diverse requirements (see Fig. 1). The Next Generation Mobile Network (NGMN) Alliance defines a network slice as a set of network functions and associated resources, forming a complete virtualized end-to-end logical network meeting certain network characteristics required by the associated service [1, 2, 16]. Namely, slices will provide virtualized resource separation for different services, while still allowing for statistical multiplexing of the resources.

An anticipated challenge is managing a large number of tenants, each with multiple services, resulting in separate slice instances. Each such instance may have unique Service Level Agreement (SLA) requirements in terms of bandwidth, latency, reliability, mobility, and security. Each slice can contain multiple bearers from multiple User Equipments (UEs)¹, and each bearer can have a Guaranteed Bit Rate (GBR)² or a non-GBR service.

The complexity of management and orchestration will increase with 5G slicing. As illustrated in Fig. 1, a Radio Access Network (RAN) slice broker (to which we will refer to as a **broker**) is used to manage and orchestrate the slice life cycle [23]. The broker monitors each slice's SLA and predicts its future RAN resource usage. The prediction is utilized to dynamically provision resources to slices. Admission control decisions are based on the slice priority

 $^{^1\}mathrm{A}$ bearer is defined as a path for the traffic with a common QoS from a UE to the Packet Data Network Gateway.

 $^{^2{\}rm GBR}$ bearers have bandwidth guarantees (e.g., min throughput, max throughput, packet delay variation) from the LTE network.

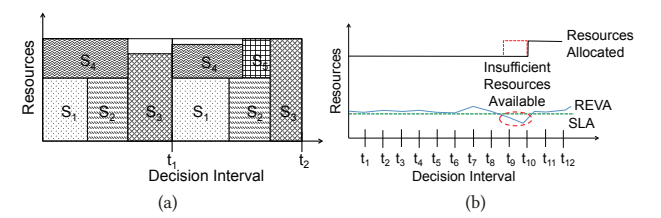


Figure 2: (a) An example of provisioning resources to slices which is based on the broker's admission control decisions, where in the second decision interval a 5th slice is admitted. (b) An example of monitoring REVA for a single slice and the corresponding dynamic resource provisioning.

and resource requirements. For example, in Fig. 2(a) during the first two decision intervals four and five slices are admitted, respectively. Slice admission control algorithms that take into account given RAN usage have been developed based on solutions to the multidimensional knapsack problem [7, 25].

Efficiently utilizing the RAN resources is crucial to enable multiplexing gains and cost effectiveness for service providers [19]. Therefore, an accurate prediction model of the usage must be developed to efficiently utilize the RAN. An overestimation in the amount of allocated resources results in a decrease in revenue for the service provider, while underestimation results in SLA violations.

Specifically, the paper has two related objectives. The first is to develop a metric that measures the amount of Physical Resource Blocks (PRBs) available to very active bearers for each slice. The metric could be easily used for slice provisioning. The second objective is to develop an accurate and short time scale prediction model of that metric. Once the prediction is obtained, the broker can use each slice's predicted PRB usage for slice provisioning.³

Accordingly we define a new metric, REVA, that precisely measures the average amount of wireless Physical Resource Blocks that the RAN scheduler can allocate to Very Active bearers (see Sec. 4). The amount of resources given to each bearer in a slice is determined by the RAN scheduler. The Very Active (VA) bearers are those that attempt to obtain more than their fair share of the PRBs that are available from the scheduler. A broker determines the amount of PRBs to allocate to each slice in order to satisfy the SLA (e.g., a slice's SLA may require a minimum video quality for a remote surveillance camera). Since the RAN scheduler reserves PRBs for each GBR bearer (e.g., voice conversation), the REVA metric focuses on measuring the PRB usage of the non-GBR bearers in a slice. For example, in Fig. 2(b) when REVA falls below the SLA in decision interval t_9 , it reveals that there are insufficient available PRBs for VA bearers. The slice provisioning algorithm would use this information to increase the total amount of PRBs allocated to that slice.

Due to the lack of relevant data and while 5G systems are still undergoing standardization and development, we design and evaluate a model for short term (single to tens of seconds) REVA prediction **using a custom-designed experimental LTE testbed** (see Sec. 5). The scheduler in the testbed is augmented with a thin layer to compute REVA in real time⁴ and we use a single Quality of Service (QoS) class identifier (QCI) per slice. The testbed was used

to collect traces of hundreds of hours of RAN resource allocation under a variety of network usage patterns. We used one, two, and three overlapping periodic time patterns to emulate the temporal patterns that occur in cellular networks [29].

The data collected from the testbed is used to develop and evaluate the prediction models for REVA (see Sec. 6). Current time series models [6, 13, 26] are inadequate for multistep prediction of network resource usage over a short time scale. These models are designed for predicting one step into the future, but there is a need for higher accuracy over multiple time steps for dynamic provisioning and other network optimization techniques (e.g., VM migration). Therefore, we design a modified Long Short Term Memory (LSTM) model, X-LSTM, to improve prediction accuracy. To evaluate the performance (see Sec. 7), we use X-LSTM to predict REVA tens of seconds in advance. We show that the gains of X-LSTM over traditional models such as Autoregressive Integrated Moving Average Model (ARIMA) and LSTM neural networks increase as the number of components in the time pattern increases. Given time patterns composed of one, two, and three independent semi-periodic components, X-LSTM outperformed ARIMA and LSTM by 10%, 22%, and 31% respectively. We show that X-LSTM achieves accuracy predictions of over 91%.

To evaluate the impact of each prediction model on slice provisioning, we introduce a simple slice provisioning algorithm. The algorithm exploits the prediction models to minimize cost for service providers. The cost is measured by the amount of over-provisioned PRBs and violating the SLA. We show that X-LSTM offers the service provider a greater than 10% cost reduction compared to ARIMA and LSTM.

2 RELATED WORK

Network Slicing: Architectural aspects of 5G RAN slicing are developed by the 5G NORMA project [4] within 5G-PPP, by utilizing Software Defined Networks and Network Function Virtualization. Wireless RAN virtualization will offer greater flexibility for network infrastructure operators, while also adding benefits to their customers (typically called tenants [21]). By enabling RAN virtualization, Mobile Network Operators can share common RAN resources leading to reduced costs and increased energy efficiency. The concept of network virtualization will enable infrastructure as a service for end to end networking [1]. An optimization framework was developed in [18] for resource allocation of network bandwidth and cloud processing. A network slice broker will enable mobile operators to request and lease infrastructure dynamically [23]. Orion was developed to enable dynamic virtualization of the base station [9]. In [7, 25], the authors develop an admission control decision algorithm for RAN slice requests based on the knapsack problem and propose solutions using a greedy algorithm and online-reinforcement learning. The resource efficiency and cost-effectiveness of resource management in network slicing is studied in [19]. Slice overbooking has been shown to maximize the revenue of mobile operators with minimal impact of SLAs [22].

Cellular Traffic: Recent work has characterized and modeled city wide traffic in cellular networks [29, 30, 32, 35, 36], where congestion is characterized by measuring the traffic load. In [11], the authors improve on previous congestion metrics by also including

³Slice admission control is out of the scope of this paper and is for future work.

⁴We expect that the additions to the scheduler and the REVA metric will be applicable to 5G schedulers.

round trip times. In [17] a single cell load measure is defined as a combination of the number of connected bearers, achieved throughput, and percentage of total PRBs per bearer. In [28] congestion is characterized via skewness of measured aggregate throughput.

Network Analytics: Numerous research efforts have been devoted to improving network performance using network analytics. In [5, 27] traffic congestion and mobility is predicted across a university WLAN network. Improvements for adaptive video streaming performance over LTE are studied in [33, 34, 37] where the LTE bandwidth is estimated by monitoring the broadcast messages or LTE bandwidth availability is given.

Time Series Modeling: Statistical and machine learning models for forecasting time series have received significant attention. Common statistical models are ARIMA and the Seasonal ARIMA (SARIMA) models [6, 26]. Neural Networks (NNs), a popular model in machine learning, are used to approximate non linear multivariate functions. Recurrent Neural Networks (RNNs) is a NN that uses feedback from previous steps. A specific type of RNN is an LSTM NN, which has memory cells to maintain information for longer periods [13]. Additional work has been done to improve the performance of LSTMs for specific applications [8, 10, 20].

3 WIRELESS RAN

In this section, we provide background on RAN resource allocation and then discuss the limitations of the existing metrics available for monitoring resource utilization. Note that we use LTE terminology while describing and evaluating our methods, but they should be applicable to 5G schedulers which are currently in development.

3.1 Background on RAN Resource Allocation

3GPP defines wireless resource allocation in the time and frequency domains. LTE and LTE Advanced utilize a resource allotment unit called a PRB. A PRB consists of 180 kHz in the frequency domain and one slot of 0.5 ms in the time domain. Every Transmission Time Interval (TTI) (1 ms in LTE), the scheduler distributes the available PRBs for the Downlink (DL) and Uplink (UL) among LTE bearers. The total number of PRBs assigned depends on the number of TTIs and the system bandwidth configuration. According to the LTE standard, there are 6 PRBs per TTI for 1.4 MHz configuration to 100 PRBs for 20 MHz configuration [2].

The scheduler at the base station (eNodeB) uses channel condition information received periodically from the UEs to assign Modulation and Coding Schema (MCS) to the allocated PRBs. This essentially determines the number of bits transmitted using the allocated PRB. Using a higher MCS with poor channel conditions leads to data loss and requires using more PRBs for retransmissions. In good channel conditions, using a lower MCS leads to unnecessarily reduced throughput. RAN scheduling algorithms are optimized to determine the best MCS assignment for each allocated PRB. In the time domain, the schedulers also make decisions regarding how often PRBs are assigned to a specific bearer.

The LTE standard defines scheduling priorities or QCIs to address the different scheduling rules for the different classes of service [3]. Each QCI has its own associated QoS characteristics (e.g., priority, guaranteed (or not) bit rate, packet delay budget, and packet error loss rate. QCIs reserved for GBR service have the scheduler attempt

to ensure certain guaranteed bitrate for the bearer. For example, QCI 1 is typically reserved for Voice over IP traffic. QCIs designed for non-GBR traffic typically use weighted or max-min fair share scheduling algorithms for PRB allocation [3]. Max-min fair share algorithms assign users with a small demand the resources that they need and distribute the remaining resources evenly to large users.

3.2 RAN Resource Utilization Metrics

The broker allocates PRBs based on the SLA of each slice. In order to get better insight into provisioning resources, it is important to understand how bearers in that slice are currently utilizing the resources. In addition, it would be insightful to separate PRB usage and user channel conditions. Each have an essential role in the throughput and latency of individual UEs. RAN usage has been studied by several previous research efforts [11, 17, 28–30, 35]. However, they specifically do not focus on the application of RAN slicing. Below are examples of metrics that are not adequate for a broker.

- Aggregate percent of available PRB utilization per second by the scheduler [17] There is no sense of fairness and relation to per bearer SLA. A single greedy application such as FTP can utilize close to 100% of all PRBs in the LTE RAN, if there are no other bearers served by the RAN. Clearly, the RAN serving just a single client is not congested, and if a second FTP client joins, the scheduler would allocate to it roughly half of the available PRBs.
- Aggregate throughput of all bearers [29, 30, 35] The metric is inadequate for the same reasons given above. A single FTP bearer in perfect channel conditions can utilize close to 100% of all PRBs.
- Metrics based upon latency or throughput of individual or groups of bearers [11, 28] - These metrics are inadequate due to the reasons below:
 - Bearer throughput depends on channel conditions. Low throughput or high latency of bearer(s) may not result from RAN congestion but could result from poor channel conditions of the respective bearer(s).
 - Low throughput may be a function of applications usage characteristics. Specific applications may not need a lot of network resources (e.g., Voice over IP, low resolution video, and instant messaging).
- Number of users served by the RAN Such a metric does not take into account RAN resource consumption by individual bearers. A RAN serving a large number of VoIP or other low volume bearers is not necessarily congested.

4 RAN RESOURCE ESTIMATION

In this section we outline the design objective for a prediction model along with the REVA metric. We then describe the definitions needed for REVA, and the algorithm for its computation.

4.1 Objective

Our objective is to develop a metric, REVA, that can be used by a broker to efficiently measure, predict usage, and provision slice resources. We represent REVA as y_t throughout the remainder of the paper. We assume the broker has a history of T decision

intervals of the series: $\mathbf{y_{t-1}} = (y_{t-1}, y_{t-2}, ..., y_{t-T})$. A prediction model f uses the history $\mathbf{y_{t-1}}$ to predict s decision intervals ahead: $\hat{y_t}, \hat{y_{t+1}}, ..., \hat{y_{t+s-1}} = f(\mathbf{y_{t-1}})$. The goal is to develop a prediction model for y_t that has a minimal prediction error ϵ_t :

$$y_t = f(\mathbf{y_{t-1}}) + \epsilon_t. \tag{1}$$

The REVA metric is developed as follows:

- A function of the available resources that is independent of: (i) channel conditions of the bearers; (ii) the application behavior and throughput needs of individual user bearers; (iii) transport protocol (e.g., TCP, QUIC, UDP, or raw IP); (iv) bearer throughput or roundtrip time. This would allow for scheduling slices based on the required PRBs.
- The average number of PRBs used by the bearers that attempt to obtain more than their maximal fair share of PRBs (defined as very active bearer in Definition 4.2). These are the bearers that need to be monitored to ensure SLAs.
- A method for precise and direct computation of available bearer throughput per slice. When combining the amount of average PRBs (\$\overline{PRB_i}\$) with individual channel bearer conditions (\$b_i\$), it allows for easy derivation of the wireless throughput available to a very active bearer \$i\$. The throughput can be computed as:

$$R(b) = \overline{PRB_i} \cdot C(b_i) \tag{2}$$

where $C(b_i)$ is the average number of useful bits per PRB for bearer i [31]. The forecast of the UEs channel quality can be used to estimate the MCS [24]. Table 1 illustrates the average throughput given a variety of PRB rates along with the user's MCS. For each PRB range, 3 MCS values are provided along with the corresponding resulting max throughput.

4.2 Definitions

We introduce the following definitions prior to defining REVA. Without loss of generality, we assume one or more QCIs per slice.

Definition 4.1. Active bearers for a non-GBR QCI m are bearers that use on average γ PRBs per second (e.g., $\gamma = 30$)⁵. Active bearers can be broken down into two groups: Very Active and Less Active.

Definition 4.2. Very Active (VA) bearers for a non-GBR QCI *m* are those that continuously attempt to obtain more than a maximal fair share of PRBs that are available from the scheduler for a given duration of time.

Definition 4.3. Less Active (LA) bearers for a non-GBR QCI *m* are the active bearers that are not VA.

Examples of VA bearers are FTP and HTTP adaptive streaming video. Examples of LA bearers are web browsing and viewing social media. An example of a non-active bearer is a smartphone application that periodically performs keep-alive handshakes and receives push notifications. Bearers for each slice are classified into VA and LA based upon PRB resource consumption.

REVA is now formally defined as the following:

Table 1: Throughput for PRB rate along with the UE's MCS.

Average PRBs/sec	MCS	Max Throughput(kb/sec)	
0-500	8,19,27	70,180,310	
500-1000	8,19,27	140,360,630	
1000-2000	8,19,27	280,720,1260	
2000-3000	8,19,27	420,1080,1900	
3000-5000	8,19,27	700,1800,3150	

Table 2: Notation.

Symbol	Semantics		
Stotal	Total number of PRBs/sec available		
	to a slice over interval Δt		
δ	Fraction of control plane PRBs		
	(typically 0.01 or 0.02)		
w_m	Proportional fair weight for QCI_m		
$RPRB_m$	Reserved PRBs for QCI_m		
$\vec{B_m}$	Vector of PRBs of active bearers at QCI_m		
\vec{R}_m	Vector of PRBs of unclassified active bearers at QCI_m		
$\vec{L}\vec{A}_m$	Vector of PRBs of LA bearers at QCI_m		
N_m	Number of active bearers at QCI_m		
NR_m	Number of unclassified active bearers at QCI_m		
U_m	Number of PRBs used by LA bearers at QCI_m		
I_m	Fair share of PRBs at QCI_m		

Procedure 1 Aggregate available PRB Rate

```
1: procedure S_m

2: S = S^{\text{lotal}}(1 - \delta) - \sum_{j \le 4} PRB_j

3: if Proportional Weighted Share Scheduling then

4: S_m = S - \sum_{5 \le j \le 9, j \ne m} min(\overline{PRB_j}, S \cdot w_j)

5: if Strict Priority Scheduling then

6: S_m = S - \sum_{5 \le j \le m} S_j - \sum_{j \ge m+1} RPRB_j

return S_m
```

Definition 4.4. REVA for a slice is defined per QCI and traffic direction (DL or UL) as: available <u>Re</u>source rate (in PRBs/sec) for an ideal 'Very <u>Active</u>' bearer.

REVA determines the number of PRBs that a VA bearer at a given QCI can obtain. REVA specifically focuses on non-GBR bearers since, for GBR bearers a guaranteed amount of resources are allocated. The GBR service class guarantees the throughput and therefore the amount of PRBs allocated to a GBR bearer depends upon bearer channel conditions which typically varies in time. Notice that we use 1 second (1,000 TTIs) as the time interval. For low latency slices, one can use a smaller time interval (e.g., 20 to 100 TTIs).

The algorithm to calculate REVA appears in Algorithm 1. Bearers are categorized in an iterative way similar to the max-min fair share algorithm. In each iteration, LA bearers are those that use less than their fair share of the resources remaining. We define $S^{\rm total}$ as the total number of PRBs/sec available to a slice. For example, for a slice with 10 MHz bandwidth, $S^{\rm total}=50,000$ PRBs/sec. The available PRBs for the slice is $S^{\rm total}(1-\delta)$, where δ represents a fraction of control plane PRBs.

In this section, we assume that the slice includes multiple QCIs and we compute the REVA metric for each non-GBR QCI. Algorithm 1 consists of two steps:

 $^{^5}$ 30 PRBs limits the max throughput of a bearer to \sim 1 KBps with channel conditions appropriate for 16QAM modulation. This parameter can vary based on the service type of the slice.

Algorithm 1 REVA Computation

```
1: Initialize \delta, S^{\text{total}}

2: for m = 5 : 9 do

3: Initialize \vec{B_m}, N_m, L\vec{A_m}

4: B\vec{R}_m = \vec{B_m}, NR_m = N_m, NR_m^{\text{prev}} = 0, U_m = 0

5: Calculate S_m (Procedure 1)

6: while do NR_m \neq NR_m^{\text{prev}}

7: NR_m^{\text{prev}} = NR_m

8: I_m = \frac{S_m - U_m}{max(1,NR_m)}

9: Update B\vec{R}_m, NR_m, U_m, L\vec{A}_m

10: REVA(m) = \frac{S_m - U_m}{VA_m}
```

- Compute available PRB rate per QCI of the slice. (line 5 of Algorithm 1, Procedure 1)
- For each QCI, classify the slice bearers into VA and LA based upon their PRB consumption. Then, compute the REVA value. (lines 6-10 of Algorithm 1)

 $\vec{B_m}$ is the vector of PRB rates for all the active bearers at QCI_m . Initialization is done by assigning N_m as the total number of active bearers at QCI_m . $\vec{BR_m}$ is the vector of PRB rates for all the active bearers that have not been classified yet, and is initially set to $\vec{B_m}$. NR_m is denoted as the number of active bearers that have not been classified yet and is initially set to N_m . U_m is the number of PRBs used by LA bearers, and is initially 0. $\vec{LA_m}$ is the vector of PRB rates for bearers that are classified as LA, and initially it is empty.

The next step of Algorithm 1 is to estimate the amount of available PRBs for non-GBR QCI_m (Procedure 1).

Procedure 1 first adjusts for control PRBs and then removes the PRB rate for all the GBR bearers in line 2. The next computation performed depends upon the scheduling schema used across QCI classes. If proportional weighted share scheduling is used, S_m is set based on the minimum of the fair share requirement or the amount of traffic required for that QCI level. In the case of priority scheduling, the amount of resources for that QCI level is calculated based on the amount of resources for higher priority QCI levels and the amount of Required PRBs (RPRB) for lower priority QCIs. The minimum number of resources for lower priority QCIs is used to ensure that even lower priority QCIs are not starved.

Algorithm 1 continues by iteratively eliminating LA bearers. In each iteration, the amount of fair share of PRBs, I_m , is calculated. LA bearers are those that use less than I_m . The amount of PRBs used by LA bearers, U_m , is updated accordingly. After eliminating LA bearers, the amount of unclassified active bearers and the vector of PRBs of those bearers are updated, NR_m and $B\vec{R}_m$, respectively. Iterations continue until either no additional LA bearers are added $(NR_m^{\text{prev}} == NR_m)$, or 0 or 1 non-LA bearers remain. Eliminated bearers are LA, and remaining bearers are classified as VA. The resulting REVA level is computed for each QCI m. Each slice will have at least 1 VA bearer by definition. Therefore, if 0 non-LA bearers remain, then the LA bearer with the largest number of PRBs becomes VA.

Table 3: REVA computation example.

Iteration	NR_m	U_m	I_m	LA UEs
0	20	0	2,450	12-20
1	11	1,620	4,307	8-20
2	7	16,120	4,697	5-20
3	4	25,620	4,845	3-20
4	2	39,120	4,940	2-20
5	1	44,020	4,980	2-20

4.3 Computation Example

Consider a scenario where 20 UEs are served by a 10 MHz slice (50,000 PRBs/sec) with $\delta=0.02$ and each UE has a single DL bearer at QCI 9. The PRBs over the past 1 second are assigned as follows (all units in PRBs/sec): UE1-5000, UE2-4900, UE3-4800,..., UE9-4200, UE10-3000, UE11-3000, UE12-20 each have 180 PRBS/sec. For example, in iteration 0 there are initially 20 active bearers, with $S_m=49,000$. The fair share would be $I_m=2,450$ PRBs, but UEs 12 to 20 use less than that amount and should be classified as LA. The amount of PRBs used by the LA bearers, U_m , would then be set to 1,620 with 11 remaining active bearers for iteration 1. The algorithm would then operate as shown in Table 3. After 6 iterations there is 1 VA UE, resulting in a REVA value of 4,980 PRBs/sec.

There is one UE that is using its maximal share of the PRBs and the other UEs do not require additional resources. This can be converted into throughput based on the UE's MCS. The slice broker can then update the slice's PRB allocation accordingly.

5 EXPERIMENTAL DATA COLLECTION

Due to the lack of data from service providers, we built an experimental LTE testbed to collect data and calculate the REVA metric. PRB distribution per bearer with ≤ 1 second granularity is unavailable from deployed eNodeBs. Hence, we designed a lab LTE network with synthetic loads. The collected data is used in Sec. 6 to train forecasting models and in Sec. 7 to evaluate the impact prediction accuracy has on dynamically allocating resources. In this section we describe the experimental setup and the data collection process.

5.1 LTE Testbed

The experiments were performed using the lab testbed configuration depicted in Fig. 3. The LTE eNodeB was configured with a 10 MHz bandwidth using 700 MHz wireless spectrum (LTE band 13). All UE minicomputers were connected to LTE Remote Radio Heads (RRHs) via LTE USB modems using Radio Frequency (RF) cables and splitters. An RF impairment tool with two input and two output ports was used to emulate a variety of radio conditions for two groups of UEs.

Slices were emulated by using different QCIs, with separate Access Point Names (APNs) configured for each slice. For the purpose of this paper we focused on predicting REVA of a non-GBR slice at QCI 9. We built an LTE load generator consisting of 15 UEs configured for QCI 9 and 3 UEs configured for QCI 3 (GBR). The operation of the load generator was controlled via scripts by a load generator controller connected to the UEs over Ethernet LAN. In each experiment, the non-GBR UEs were running FTP download over LTE in a continuous loop. The scripts also controlled GBR UEs to start/stop

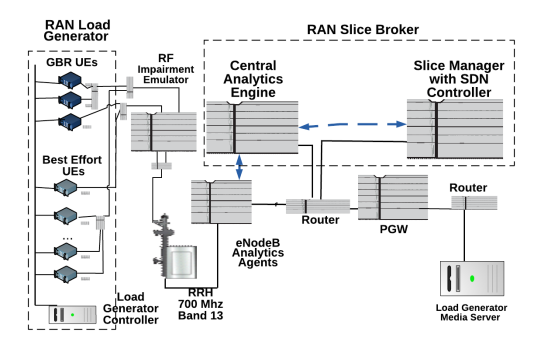


Figure 3: Lab Configuration Setup. The LTE eNodeB scheduler calculates REVA which is forwarded to Central Analytics Engine to compute optimal policy action. The Central Analytics Engine sends the action to the Slice Manager for enforcement. Additional components (MME, SGW, HSS, PCRF) are left out for simplicity.

FTP download over LTE to emulate multiple independent patterns for the non-GBR slice.

We enhanced the LTE eNodeB scheduler by adding a thin layer to instantaneously compute REVA. The LTE eNodeB scheduler sends data digests every second in the form of the REVA metric per QCI and per slice to the Central Analytics Engine (CAE) via a dedicated out-of-band connection. The CAE performs instantaneous REVA data smoothing and further processing of the smoothed data. The predicted REVA metric is processed by the CAE policy engine to suggest an optimal policy for resource allocation. The CAE then sends this suggestion to the slice manager for enforcement.

5.2 Data Collection

The REVA metric (Section 4) is calculated at the eNodeB Scheduler. It records per bearer PRB distribution data every TTI (1 millisecond), and aggregates per bearer data into bins of time duration Δt (e.g., $\Delta t=1$ second or $\Delta t=100$ milliseconds). At the end of each Δt interval, it performs the computation described in Algorithm 1 (Section 4) and sends data digest per QCI level to the analytics engine. Our measurements indicate that executing Algorithm 1 every 1 second with approximately 500 active bearers adds less than 1% to eNodeB CPU utilization. The algorithm's complexity is $O(k^2)$, where k is the number of users. Performing preprocessing of the data at the agent instead of sending the raw scheduler data every 1 millisecond, reduces the amount of data transfer by a factor of more than 1000.

The original REVA data has a high variance over short windows due to fluctuations in the TCP client behavior. To rectify this issue we smoothed the data to reduce the noise fluctuations. Smoothing is done by looking at a window size of 10 seconds and eliminating the minimum and maximum values to remove potential outliers. The minimum remaining value of REVA is chosen. We focus on the minimum opposed to other metrics (e.g., mean, median, max) to ensure that current slices have enough resources and to prioritize current slices over incoming new slices.

In this paper, we discuss 3 time series sets collected from the testbed. [29] shows that there are temporal patterns of cellular traffic at time scales on an hourly, daily, and weekly basis. We vary

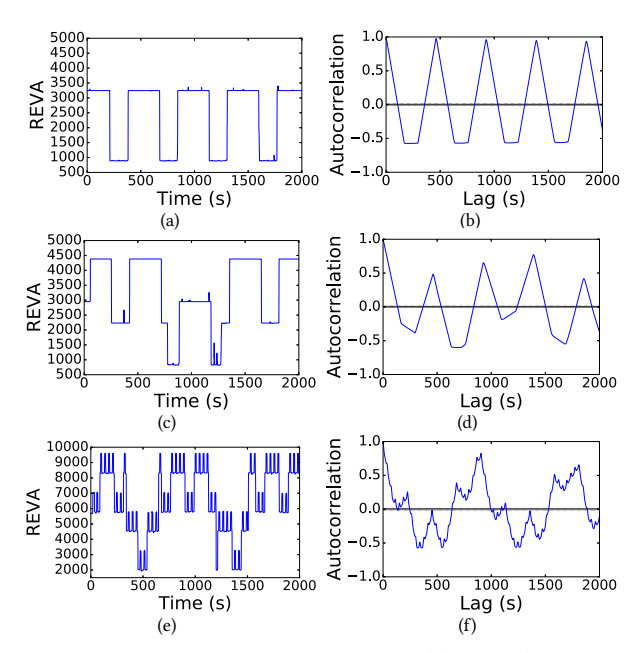


Figure 4: Experimental Data Collected (a) Set 1, (b) Set 1 autocorrelation, (c) Set 2, (d) Set 2 autocorrelation, (e) Set 3, (f) Set 3 autocorrelation.

the number of overlapping temporal patterns from 1 to 3 to emulate similar situations.

The data sets consist of the 15 non-GBR clients using FTP, and were collected for roughly 18 hours. The first data trace contained one periodic GBR client and is referenced as Set 1 and viewed in Fig. 4(a). This resulted in a simple square pattern with small variations and can be used for baseline evaluations of the prediction models. The second data set had two varying GBR clients that used FTP and is referenced as Set 2 and viewed in Fig. 4(c). Three GBR clients periodically used FTP to create a three pattern overlay profile for Set 3 (Fig. 4(e)).

The Autocorrelation Function (ACF) is used to analyze the potential predictability of a time series. ACF is the correlation of a signal with a time lag l version of itself. The results of ACF give insight into how much information from the past can be used to predict future values. Figs. 4(b), 4(d), 4(f) show ACF at a time lag of l=0,1,...,2000 for REVA in Sets 1,2, and 3, respectively.

The periodic nature of ACF for Set 1 shows spikes that do not decay. It also reveals that the underlying data should have a high predictability. The ACF of Set 2 shows a stong autocorrelation for the first 100 time lags with additional significant correlation at later time lags. The medium correlation values reveal a time series that should have moderate predictability. The ACF of Set 3 is not smooth like the previous two functions. In addition, there are not as many peaks in the ACF, meaning that this data set should be the most difficult of the three to predict.

6 MACHINE LEARNING MODELS

A precise prediction model allows a broker to utilize the RAN more effectively. Therefore, there is a need for reliable and short term prediction of the slice resource utilization. Current time series

models are designed for predicting one step into the future and do not perform well when predicting multiple steps at a time. Our design objective is to forecast REVA for the next 30 seconds with prediction intervals of 5 seconds. The forecasting function $f(\mathbf{y}_{t-1})$, will provide a forecast for $y_{t+5}^{-}, y_{t+10}^{-}, y_{t+15}^{-}, y_{t+20}^{-}, y_{t+25}^{-}, y_{t+30}^{-}$. The first 60% of each time series is used as training data, the next 20% for validation, and the final 20% for testing. We begin this section with a description of the time series models used as a baseline: ARIMA and LSTM. We then describe the architecture of the X-LSTM model designed to solve this problem.

6.1 ARIMA

One of the most popular statistical methods for time series analysis is the ARIMA model [6]. The ARIMA model assumes that future values are a linear function of previously observed values and random noise. The ARIMA model can be modeled as ARIMA(p,d,q).

The data used to train the ARIMA model was the 5 second averages of the smoothed data. The ARIMA model was implemented in Python using the Statsmodel package. Optimizing the performance of the ARIMA prediction model requires tuning of the parameters p, q, and d. The optimal model was selected by a grid search while varying the parameters for p, q, and d between 0 and 3. The parameter setting that gave the minimum RMSE for the validation data was (p,q,d)=(1,0,1) for both data sets. To obtain a 30 second prediction, there were 6 steps of prediction done at a time. The ARIMA model parameters are retained for every batch of multistep prediction.

6.2 LSTM

Recurrent Neural Networks (RNNs) differ from traditional Feedforward Neural Networks (FNNs) in that they contain feedback loops to allow information to propagate from previous steps. Feeding information from previous steps into the next step allows for a deep neural network architecture without computing and storing as many parameters. Therefore, these models are ideal neural network architectures for time series prediction. One of the major problems with traditional RNN is that it does not store information for long periods of time due to the vanishing gradient problem [12]. A type of RNN specifically designed to understand long term dependencies is an LSTM [13].

We implemented the LSTM neural network in Python on Keras using the Tensorflow backend. It contains a single recurrent layer with a linear layer. Validation data was used to tune the performance of a variety of neural network architectures. The architecture chosen for testing uses a single LSTM layer with 100 hidden neurons, and a dense output layer to predict the output congestion level. The LSTM uses a history of the previous 80 timesteps to predict the next step. The learning rate was set to $\alpha=0.005$. The input data is the 5 second averages of the RAN congestion. In theory, LSTMs can store memory for an infinite number of timesteps, but, as the number of timesteps increases it creates more computation complexity to tune the parameters for back propagation. In implementation the Truncated Back Propagation Through Time (TBPTT) method is used to limit the number of memory steps [15].

For multistep prediction (Multistep LSTM), an iterative procedure is used with T set to 80. For the first prediction the real past

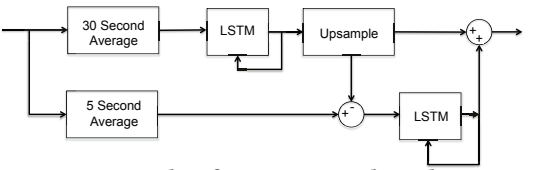


Figure 5: An example of X-LSTM machine learning architecture used for the experimentally collected data. This X-LSTM architecture contains two phases, one at a time scale of 30 seconds and the next at 5 seconds.

80 timesteps are used. For the second prediction, 79 real timesteps are used along with the previously predicted value. This continues until the 6th prediction is done with 75 real values and the previous 5 predicted values.

6.3 X-LSTM

We develop X-LSTM as an extension of LSTM. It is based on the idea of ARIMA and the X-11 statistical method. X-11 is an iterative process that decomposes time series data into seasonal data patterns. This method combined with the prediction of an LSTM improves results over standard methods. We break the method into two phases as can be seen in Fig. 5.

The X-LSTM model uses multiple LSTMs, each with a different time scale. It filters out higher order temporal patterns and uses the residual to make additional predictions on data with a shorter time scale.

We implemented each LSTM neural network of X-LSTM in Python using Keras with the Tensorflow backend. Each LSTM block contains a single recurrent layer with 100 hidden neurons with a dense output layer. For each LSTM block 80 timesteps were used. The learning rate was set to $\alpha=0.005$.

For our experimental data, the first phase is done at a 30 second time level. The first LSTM block makes predictions for the average over the next 30 seconds, y_{t+30} . The goal of the next phase LSTM is to make predictions for the time series of the residuals $(y_t - y_{t+30})$ at a higher granularity. For our evaluation, a second phase with a time scale of 5 seconds was used. The residual values for Sets 1, 2 and 3 are seen in Figs. 6(a), 6(c), and 6(e), respectively. Looking at the autocorrelations, in 6(b), 6(d), 6(f), reveals that the residual data has information from previous time lags that can be used to improve the prediction accuracy.

The first step is to make a prediction for the average over the next 30 seconds. The second LSTM phase predicts the residual $(y_t - y_t\hat{}_{+30})$ on a granularity of 5 seconds. It is used for multistep prediction in an iterative procedure for 6 steps. The 6 predicted values are then added back to the predicted 30 second average in order to predict REVA at $y_t\hat{}_{+5}, y_t\hat{}_{+10}, y_t\hat{}_{+15}, y_t\hat{}_{+20}, y_t\hat{}_{+25}, y_t\hat{}_{+30}$.

The number of phases and the time scale of each phase are the additional tuning parameters for X-LSTM neural network. While each of our data sets was only collected for roughly one day, this method can be extended to longer data sets by including additional phases. Typically networks exhibit time patterns due to natural seasonal, weekly, daily, and hourly traffic variations [29]. Data can be reduced by summarizing the data into lower granularity. For example, instead of storing per second data, data can be summarized into hourly, and daily averages. Data can be stored on the granularity

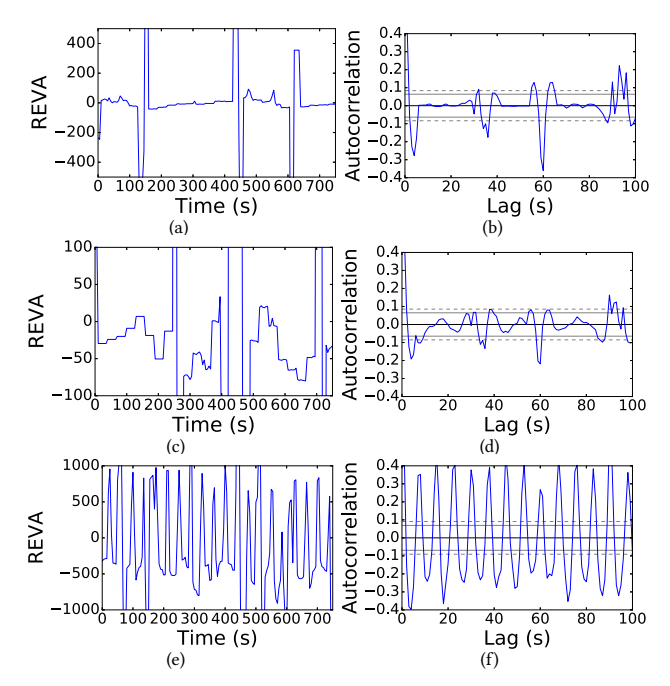


Figure 6: Residual of first phase prediction (a) Set 1, (b) Set 1 autocorrelation, (c) Set 2, (d) Set 2 autocorrelation, (e) Set 3, (f) Set 3 autocorrelation.

of seconds for the past day, per hour bases for the past month, and daily values for the past year. This can reduce the amount of data needed for prediction by over 99%.

7 EVALUATION

In this section we briefly discuss accuracy measures used for evaluation. We then analyze the prediction accuracy of each proposed prediction model. We continue with a description of a slice provisioning algorithm and design of a cost function based on the amount of over-provisioned PRBs and SLA violations. We conclude by showing how the algorithm exploits the prediction models to minimize cost for service providers.

7.1 Prediction Results

Accuracy measures used for comparison between the different time series methods include: Root Mean Square Error (RMSE), Mean Absolute Error (MAE),and Mean Absolute Percentage Error (MAPE). The true output value is y_t and the predicted value is $\hat{y_t}$ for each time t. The accuracy of each proposed method is measured by splitting the experimental data collected into three components: training, validation, and test. The training data is used to tune the machine learning parameters for each method, while the validation data determines the best parameters for each method. The test data is used to compare the performance of each model.

The prediction results on test data for Sets 1, 2, and 3 can be seen in Fig. 7, along with the resulting error measures in Fig. 8. Four different prediction models are used for comparison. The first model predicts a one step 30 second mean of the time series using a vanilla LSTM model (referred to as 30 Second LSTM). The second model is determined by the X-LSTM model. The third prediction

model uses a multistep LSTM to determine the congestion over the next 30 seconds in a granularity of 5 seconds. The fourth model uses a multistep ARIMA model to predict the congestion over the next 30 seconds in a granularity of 5 seconds.

Set 1 follows close to a periodic square wave with numerous time steps in between. The results show that all the models are able to follow the square wave relatively accurately. The multistep LSTM and ARIMA models have a more difficult time and incorporate errors from earlier steps leading to extrapolation. The prediction of the 30 Second LSTM is better able to determine the square pattern, as it has less information to store from previous periods and is only making a one step prediction. The resulting error measurements show that even on the simpler square wave pattern, our X-LSTM model outperforms the other models. It is able to learn meaningful information from the residual between phase 1 and phase 2.

The second best model, 30 Second LSTM, gives a MAPE of 7.68% and an RMSE of 312, while the X-LSTM model gives a MAPE of 6.93% and an RMSE of 256, resulting in a 10% and 18% improvement, respectively.

Set 2 has a more complex time series which has two overlapping periodic events. All models in this data set have a higher error rate than in Set 1. The multistep LSTM has a difficult time incorporating the many variations it learned from the two overlapping patterns. When creating multistep predictions the errors continue in a positive or negative direction causing a sawtooth pattern. The multistep ARIMA model has a higher accuracy for Set 2 than the multistep LSTM model. Phase 1 of the X-LSTM model is able to track the model, however it is often slow to update when there are large changes. The X-LSTM model is able to incorporate the residual difference and make an improvement on the phase 1 predictions. The additional benefit of X-LSTM is that when the last phase LSTM needs to predict multiple steps, the bias of the prediction is reduced.

The second best model is again, 30 Second LSTM, which has a MAPE of 8.11% and an RMSE of 353. The X-LSTM model has a MAPE of 6.36% and an RMSE of 304, resulting in a 22% and 14% improvement.

The most challenging set to model due to its three overlapping periodic patterns is Set 3. The result is a lower level accuracy across all models. There is a strong residual component that has high ACF values. This allows the second phase of X-LSTM to improve upon the accuracy of the first phase and thus reduce the prediction error. The multistep ARIMA and LSTM models in this situation perform significantly worse than X-LSTM.

The MAPE of the multistep LSTM is 13.07% and for the LSTM predicting 30 second averages it is 13.03%. The X-LSTM is able to outperform these models by 31% with a MAPE of 8.99%.

7.2 Slice Allocation

We evaluate the impact that forecasting accuracy has on slice resource utilization. The REVA metric allows for easy adjustment of slice provisioning by using the difference between REVA and the SLA. The value can be used to estimate the amount of additional resources the slice should be allocated to satisfy the SLA or the amount of PRBs that should be removed while still satisfying the SLA.

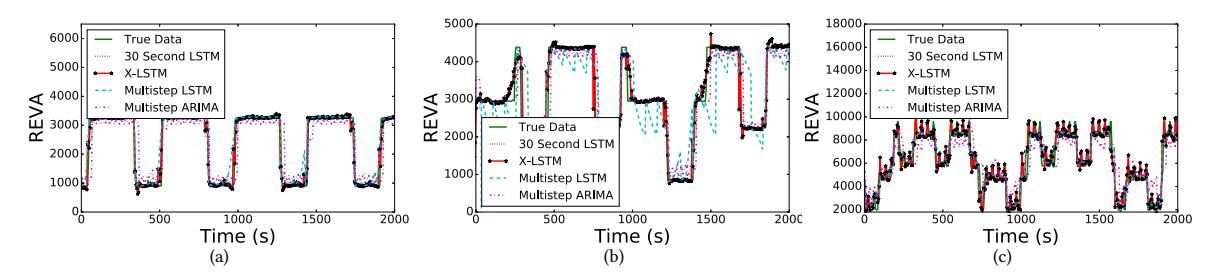


Figure 7: Results obtained by various prediction models: (a) Set 1, (b) Set 2, (c) Set 3.

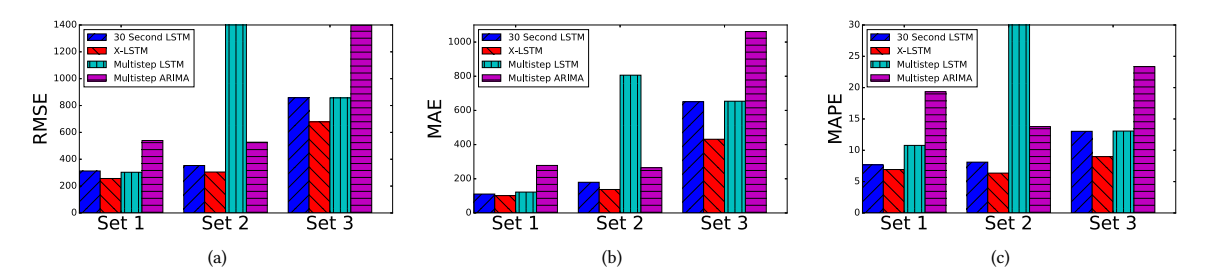


Figure 8: Prediction errors for Sets 1,2,3 illustrated in Fig. 7: (a) RMSE, (b) MAE, (c) MAPE.

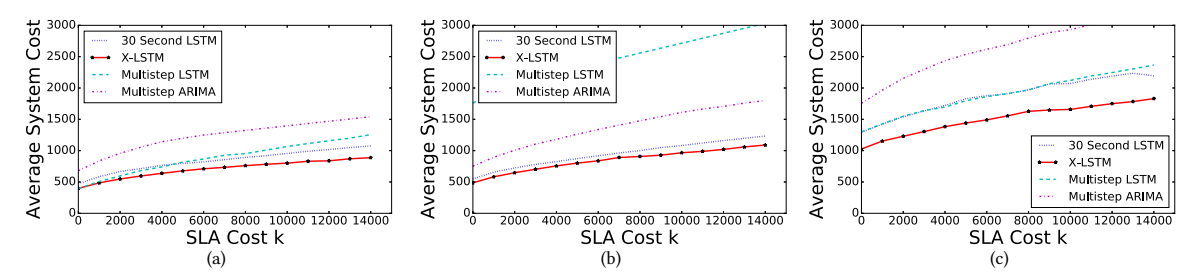


Figure 9: Average system cost vs. SLA cost K for various prediction models: (a) Set 1, (b) Set 2, (c) Set 3.

We assume that the forecasting error ϵ_t in (1) is normally distributed with a standard deviation of σ and a mean of 0, since the exact distribution of the empirical error is unavailable. This gives a Gaussian prior for the prediction model:

$$y_t \sim \mathcal{N}(\hat{y_t}, \sigma^2)$$
 (3)

We assume that assigning too few resources results in an SLA violation and incurs a penalty with cost k. Conversely, when forecasting a higher REVA value than predicted results in extra PRBs available to VA users that can otherwise be allocated to other slices. We use a one sided prediction interval h that determines the bound that should be used when assigning resources for forecast model f. We define the cost function, Γ as:

$$\Gamma(y_t) = \begin{cases} k, & \text{if } \hat{y_t} + h > y_t \\ y_t - h - \hat{y_t}, & \text{if } \hat{y_t} + h \le y_t \end{cases}$$

Accordingly, we formulate the following optimization problem to obtain the optimal h such that the system cost is minimized, given σ , $\hat{y_t}$, and k:

minimize
$$k(\hat{y_t} + h - y_t)^+ + (y_t - \hat{y_t} - h)(y_t - \hat{y_t} - h)^+$$
. (4)

Taking the expected value of the cost metric simplifies the optimization problem to:

$$\underset{h}{\text{minimize}} \quad (k + \hat{y_t})(\Phi(\frac{h}{\sigma})) - h(1 - \Phi(\frac{h}{\sigma})) + \sigma(\frac{\phi(\frac{h}{\sigma})}{1 - \Phi(\frac{h}{\sigma})}), \quad (5)$$

Where $\Phi(z)$ is the CDF of the standard normal random variable Z, and $\phi(z)$ is the PDF of the standard normal random variable Z.

7.3 Slice Allocation Efficiency

For each forecasting model, the optimal h is used for each $\hat{y_t}$ and the cost $\Gamma(y_t)$ is calculated. Fig. 9 shows the average Γ per forecasting point verses the SLA violation cost k. As k increases the optimization function weighs SLA violations more. Therefore, the number of standard deviations away the prediction interval h is increases. The optimization function causes the probability of missing the SLA to decrease from 10% to 1% (depending on the forecasting algorithm's σ , $\hat{y_t}$, and the cost k).

In data set 1, with k=0, Multistep LSTM slightly outperforms X-LSTM by less than 1%. For every other SLA cost k the X-LSTM outperforms the other forecasting algorithms. For $k\geq 5000$, X-LSTM provides more than 15%, 40%, and 15% reduction in average system cost over 30 Second LSTM, Multistep ARIMA, and Multistep

LSTM, respectively. In data set 2, X-LSTM provides more than 11%, 35%, and 60% reduction in average system cost over 30 Second LSTM, Multistep ARIMA, and Multistep LSTM, respectively. In data set 3, X-LSTM provides more than 18%, 39%, and 18% reduction in average system cost over 30 Second LSTM, Multistep ARIMA, and Multistep LSTM, respectively. Generally across the three data sets, as SLA violations increase in cost the value of X-LSTM over the other prediction models increases.

8 CONCLUSION

In order to effectively provision resources and make admission control decisions, the 5G RAN slice broker requires an accurate prediction of the required resources in a slice. We defined a new metric, REVA, that precisely measures the amount of PRBs that the RAN scheduler can allocate to VA bearers. This allows for direct derivation of wireless link throughput when coupled with channel conditions information. An experimental LTE testbed was developed to collect REVA for time series analysis. This data was then used to develop and evaluate the accuracy of time series prediction models.

We proposed and evaluated a new time series prediction model, X-LSTM, for REVA. We showed that X-LSTM provides a higher degree of prediction accuracy with a MAPE of 7.68%, 6.36%, 8.99% for Sets 1, 2, and 3, respectively. As the number of independent semi-periodic components increases from one to three in the test sets, the improvement of X-LSTM over ARIMA and LSTM increases. X-LSTM outperformed the other time series models by 10%, 22%, and 31%, respectively. In addition, X-LSTM results in more than 10% cost reduction per slice. In future work, we will further test the accuracy of X-LSTM on real world traces, and develop slice admission control algorithms for the broker, based on REVA.

ACKNOWLEDGMENTS

We thank the anonymous reviewers for helpful comments and suggestions. This work was supported in part by NSF grants CNS-1650685, and DGE 16-44869.

REFERENCES

- 2016. Description of network slicing concept. Technical Report 1. NGMN 5G Alliance.
- [2] 3GPP. 2011. Evolved Universal Terrestrial Radio Access Physical channels and modulation. TS 36.211. 3rd Generation Partnership Project (3GPP).
- [3] 3GPP. 2018. Policy and charging control architecture (Release 15). TS 23.203. 3rd Generation Partnership Project (3GPP).
- [4] 5G Infrastructure Association and others. 2017. Deliverable D3.2 5G NORMA network architecture Intermediate report. January (2017).
- [5] Haitham Abu-Ghazaleh and Attahiru Sule Alfa. 2010. Application of mobility prediction in wireless networks using markov renewal theory. IEEE Transactions on Vehicular Technology 59, 2 (2010), 788–802.
- [6] George EP Box, Gwilym M Jenkins, Gregory C Reinsel, and Greta M Ljung. 2015. Time Series analysis: forecasting and control. John Wiley & Sons.
- [7] Chia-Yu Chang, Navid Nikaein, and Thrasyvoulos Spyropoulos. 2018. Radio access network resource slicing for flexible service execution. In Proc. of IEEE INFOCOM Workshop on RS-FCN.
- [8] Junyoung Chung, Caglar Gulcehre, Kyung Hyun Cho, and Yoshua Bengio. 2014. Empirical evaluation of gated recurrent neural networks on sequence modeling. arXiv preprint arXiv:1412.3555 (2014).
- [9] Xenofon Foukas, Mahesh K Marina, and Kimon Kontovasilis. 2017. Orion: RAN Slicing for a Flexible and Cost-Effective Multi-Service Mobile Network Architecture. In Proc. of ACM MobiCom.
- [10] Felix A Gers, Nicol N Schraudolph, and Jürgen Schmidhuber. 2002. Learning precise timing with LSTM recurrent networks. *Journal of Machine Learning Research* 3, 8 (2002), 115–143.

- [11] Balázs Héder, Péter Szilágyi, and Csaba Vulkán. 2016. Dynamic and adaptive QoE management for OTT application sessions in LTE. In Proc. of IEEE PIMRC.
- [12] Sepp Hochreiter, Yoshua Bengio, Paolo Frasconi, and Jürgen Schmidhuber. 2001. Gradient flow in recurrent nets: the difficulty of learning long-term dependencies. (2001).
- [13] Sepp Hochreiter and Jürgen Schmidhuber. 1997. Long short-term memory. Neural computation 9, 8 (1997), 1735–1780.
- [14] Ekram Hossain and Monowar Hasan. 2015. 5G cellular: key enabling technologies and research challenges. IEEE Instrumentation & Measurement Magazine 18, 3 (2015), 11–21.
- [15] Andrej Karpathy, Justin Johnson, and Li Fei-Fei. 2015. Visualizing and understanding recurrent networks. arXiv preprint arXiv:1506.02078 (2015).
- [16] Gwanmo Ku and John MacLaren Walsh. 2015. Resource allocation and link adaptation in LTE and LTE advanced: A tutorial. IEEE Communications Surveys & Tutorials 17, 3 (2015), 1605–1633.
- [17] Raymond Kwan, Rob Arnott, Riccardo Trivisonno, and Mitsuhiro Kubota. 2010. On pre-emption and congestion control for LTE systems. In Proc. of IEEE VTC 2010-Fall.
- [18] Mathieu Leconte, Georgios Paschos, Panayotis Mertikopoulos, and Ulas Kozat. 2017. A resource allocation framework for network slicing. In Proc. of IEEE INFOCOM.
- [19] Cristina Marquez, Marco Gramaglia, Marco Fiore, Albert Banchs, and Xavier Costa-Perez. 2018. How Should I Slice My Network?: A Multi-Service Empirical Evaluation of Resource Sharing Efficiency. In Proc. of ACM Mobicom.
- [20] Daniel Neil, Michael Pfeiffer, and Shih-Chii Liu. 2016. Phased LSTM: Accelerating recurrent network training for long or event-based sequences. In Advances in Neural Information Processing Systems. 3882–3890.
- [21] Peter Rost, Christian Mannweiler, Diomidis S Michalopoulos, Cinzia Sartori, Vincenzo Sciancalepore, Nishanth Sastry, Oliver Holland, Shreya Tayade, Bin Han, Dario Bega, et al. 2017. Network Slicing to Enable Scalability and Flexibility in 5G Mobile Networks. IEEE Communications Magazine 55, 5 (2017), 72–79.
- [22] Josep Xavier Salvat, Lanfranco Zanzi, Andres Garcia-Saavedra, Vincenzo Sciancalepore, and Xavier Costa-Perez. 2018. Overbooking network slices through yield-driven end-to-end orchestration. In Proc. of ACM CoNext.
- [23] Konstantinos Samdanis, Xavier Costa-Perez, and Vincenzo Sciancalepore. 2016. From network sharing to multi-tenancy: The 5G network slice broker. IEEE Commun. Mag. 54, 7 (2016), 32–39.
- [24] Zulfiquar Sayeed, Qi Liao, Dave Faucher, Ed Grinshpun, and Sameer Sharma. 2015. Cloud analytics for wireless metric prediction-framework and performance. In in Proc. of IEEE CLOUD.
- [25] Vincenzo Sciancalepore, Konstantinos Samdanis, Xavier Costa-Perez, Dario Bega, Marco Gramaglia, and Albert Banchs. 2017. Mobile traffic forecasting for maximizing 5G network slicing resource utilization. In Proc. of IEEE INFOCOM.
- [26] Julius Shiskin. 1965. The X-11 variant of the census method II seasonal adjustment program. Number 15. US Government Printing Office.
- [27] R Sivakumar, E Ashok Kumar, and G Sivaradje. 2011. Prediction of traffic load in wireless network using time series model. In Proc. of IEEE PACC.
- [28] Péter Szilágyi and Csaba Vulkán. 2015. LTE user plane congestion detection and analysis. In Proc. of IEEE PIMRC.
- [29] Huandong Wang, Fengli Xu, Yong Li, Pengyu Zhang, and Depeng Jin. 2015. Understanding mobile traffic patterns of large scale cellular towers in urban environment. In Proc. of ACM IMC.
- [30] Jing Wang, Jian Tang, Zhiyuan Xu, Yanzhi Wang, Guoliang Xue, Xing Zhang, and Dejun Yang. 2017. Spatiotemporal modeling and prediction in cellular networks: A big data enabled deep learning approach. In Proc. of IEEE INFOCOM.
- [31] Xiaoli Wang, Edward Grinshpun, David Faucher, and Sameer Sharma. 2017. On Medium and Long Term Channel Conditions Prediction for Mobile Devices. In Proc. of IEEE WCNC.
- [32] Xu Wang, Zimu Zhou, Zheng Yang, Yunhao Liu, and Chunyi Peng. 2017. Spatio-temporal analysis and prediction of cellular traffic in metropolis. In Proc. of IEEE ICNP
- [33] Xiufeng Xie, Xinyu Zhang, Swarun Kumar, and Li Erran Li. 2015. piStream: Physical layer informed adaptive video streaming over LTE. In Proc. of ACM MohiCom.
- [34] Qiang Xu, Sanjeev Mehrotra, Zhuoqing Mao, and Jin Li. 2013. PROTEUS: network performance forecast for real-time, interactive mobile applications. In Proc. of ACM MobiSys.
- [35] Chaoyun Zhang, Xi Ouyang, and Paul Patras. 2017. ZipNet-GAN: Inferring Fine-grained Mobile Traffic Patterns via a Generative Adversarial Neural Network. In Proc. of ACM CoNEXT.
- [36] Chaoyun Zhang and Paul Patras. 2018. Long-term mobile traffic forecasting using deep spatio-temporal neural networks. In Proc. of ACM Mobihoc.
- [37] Xuan Kelvin Zou, Jeffrey Erman, Vijay Gopalakrishnan, Emir Halepovic, Rittwik Jana, Xin Jin, Jennifer Rexford, and Rakesh K Sinha. 2015. Can accurate predictions improve video streaming in cellular networks?. In Proc. of ACM HotMobile.